Monthly Notices
of the
ROYAL ASTRONOMICAL SOCIETY

MNRAS **464,** 840–849 (2017)
Advance Access publication 2016 September 14

doi:10.1093/mnras/stw2317

The puzzling orbital period evolution of the LMXB AX J1745.6−2901

G. Ponti,[1⋆] K. De,[1,2] T. Muñoz-Darias,[3,4] L. Stella[5] and K. Nandra[1]

[1]*Max Planck Institute für Extraterrestriche Physik, Giessenbachstrasse, D-85748 Garching, Germany*
[2]*Indian Institute of Science, Bangalore 560012, India*
[3]*Instituto de Astrofísica de Canarias, E-38205 La Laguna, Tenerife, Spain*
[4]*Departamento de astrofísica, Univ. de La Laguna, E-38206 La Laguna, Tenerife, Spain*
[5]*INAF – Osservatorio Astronomico di Roma, via Frascati 33, I-00040 Monte Porzio Catone (RM), Italy*

Accepted 2016 September 13. Received 2016 September 9; in original form 2015 November 9

ABSTRACT

The orbital period evolution of X-ray binaries provides fundamental clues to understanding mechanisms of angular momentum transfer and loss in these systems. We present an X-ray eclipse timing analysis of the transient low-mass X-ray binary AX J1745.6−2901. This system shows full eclipses and thus is one of the few objects of this class for which accurate orbital evolution studies can be carried out. We report on *XMM–Newton* and *ASCA* observations covering 30 complete X-ray eclipses spanning an interval of more than 20 yr. We improve the determination of the orbital period to a relative precision of 2×10^{-8}, two orders of magnitudes better than previous measurements. We determine, for the first time, a highly significant rate of decrease of the orbital period $\dot{P}_{\rm orb} = -4.03 \pm 0.32 \times 10^{-11}$ s s^{-1}. This is at least one order of magnitude larger than expected from conservative mass transfer and angular momentum losses due to gravitational waves and magnetic braking, and might result from either non-conservative mass transfer or magnetic activity changing the quadrupole moment of the companion star. Imprinted on the long-term evolution of the orbit, we observe highly significant eclipse leads–delays of ∼10–30 s, characterized by a clear state dependence in which, on average, eclipses occur earlier during the hard state.

Key words: accretion, accretion discs – methods: observational – binaries: eclipsing – stars: neutron – stars: winds, outflows – X-rays: binaries.

1 INTRODUCTION

Eclipse timing provides us with powerful fiducial marks to investigate the orbital period evolution in low-mass X-ray binaries (LMXBs; e.g. Chou 2014). This observable is closely associated with angular momentum variations of the system. In fact, any physical mechanism modifying the system angular momentum will inevitably modify the binary orbital period. The orbit can evolve as a consequence of mass transfer between the two stars (e.g. due to Roche lobe overflow), gravitational wave radiation (Peters 1964; Paczyński 1967; Faulkner 1971; Verbunt 1993), magnetic braking (Eggleton 1976; Verbunt & Zwaan 1981; Rappaport, Verbunt & Joss 1983), mass-loss from the companion, accretion disc winds, jets or other types of outflows (e.g. Fender, Belloni & Gallo 2004; Ponti et al. 2012), and tidal interactions between the components of the binary system.

The theory of angular momentum evolution due to mass transfer via Roche lobe overflow and gravitational wave radiation is well established and leads to quantitative predictions (Landau & Lifschitz 1958; Paczyński 1967; Faulkner 1971; Verbunt 1993). However, angular momentum losses due to emission of gravitational waves only dominate at short orbital period ($P_{\rm orb} \lesssim 2$ h), while other mechanisms, such as magnetic braking, are invoked to explain the orbit evolution at longer periods. The theory at the heart of the magnetic braking model is based on the same physical principles through which magnetic stellar winds are known to decelerate the rotation of low-mass stars (e.g. Kraft 1967; Skumanich 1972; Soderblom 1983). In synchronized binaries (typically the case of LMXBs), the angular momentum loss from the companion star is continuously re-distributed to the angular momentum of the whole binary system, therefore affecting its orbital period and binary separation (e.g. Tauris 2001). Large uncertainties are involved in the extrapolation of magnetic braking from isolated low-mass stars to the case of synchronized companion stars in LMXBs (e.g. see discussion in Knigge, Baraffe & Patterson 2011). Indeed, despite the large allowed range of model parameters (possibly translating into more than one order of magnitude on efficiency of angular momentum removal), magnetic braking often fails to reproduce measured values of the orbital period derivative, at least in the case of conservative mass transfer (Di Salvo et al. 2008; Hartman et al. 2008, 2009; Hu, Chou & Chung 2008; Burderi et al. 2010; Jain, Paul & Dutta 2010; González Hernández, Rebolo & Casares 2012, 2014). Additional mechanisms, typically involving outflows, are generally necessary

⋆ E-mail: ponti@iasfbo.inaf.it

to explain these discrepancies (Di Salvo et al. 2008; Hartman et al. 2008, 2009; Burderi et al. 2010). We also note that some of the best-monitored sources (i.e. EXO 0748−676; Wolff et al. 2009) show erratic variations of the orbital period with amplitudes of $\Delta P/P \sim 10^{-5}$ and possible trends recurring on time-scales of years-to-decades, such as those observed in e.g. Algols systems (Kreiner & Ziolkowski 1978; Hall 1989). These variations are thought to be the consequence of the torque provided by the magnetic activity of a sub-surface magnetic field in the companion star with convective envelope. The latter induces a cyclic exchange of angular momentum between the inner and outer parts of the companion star causing a change in the gravitational quadrupole moment (Applegate 1992; Applegate & Shaham 1994; Lazaridis et al. 2011).

Up to now, there are only a handful of LMXBs showing full eclipses for which a determination of the orbital period evolution has been possible (e.g. MXB 1659−29 Wachter, Smale & Bailyn 2000; GRS J1747−312 in't Zand et al. 2003; Her X-1 Staubert, Klochkov & Wilms 2009; EXO 0748−676 Wolff et al. 2009; XTE J1710−281 Jain & Paul 2011).

AX J1745.6−2901 is a dipping and eclipsing neutron star LMXB, showing type I bursts, discovered in *ASCA* data during the 1993–1994 outburst (Maeda et al. 1996). It is one of the brightest X-ray transients of the Galactic Centre region, located only ∼1.5 arcmin away from the supermassive black hole at the Galactic Centre (Kennea & Skinner 1996; Maeda et al. 1996; Hyodo et al. 2009; Degenaar et al. 2012; Ponti et al. 2015a,b). During outburst it reaches a brightness of 1–30 per cent the Eddington luminosity, alternating the hard (power-law dominated) and soft (thermal) states typically seen in 'Atoll' sources (Gladstone, Done & Gierliński 2007; Muñoz-Darias et al. 2014; Ponti et al. 2015b; see Section 6.3).

The high column density of absorbing material ($N_{\rm H} \sim 2 \times 10^{23}\,{\rm cm}^{-2}$) and the study of the blackbody radius during type I X-ray bursts suggest that AX J1745.6−2901 is located at or beyond the Galactic Centre (Maeda et al. 1996; Ponti et al. 2015a). The first determination of the orbital period was obtained by folding the eclipses detected in the 1994 *ASCA* data, yielding $P_{\rm orb} = 8.356 \pm 0.008$ h (30082 ± 29 s; Maeda et al. 1996, see also Sakano et al. 2001). Using *Suzaku* and *Chandra* observations taken between 2007 July and September, Hyodo et al. (2009) measured an orbital period of $P_{\rm orb} = 30\,063.74 \pm 0.14$ s, consistent with the previous result. Due to its transient nature, crowding and high extinction (preventing detection below ∼3 keV), the orbital evolution of AX J1745.6−2901 has not been measured yet.

Here, we study for the first time the evolution of the orbital period of AX J1745.6−2901 over an interval of more than 20 yr by using data from 15 yr of *XMM–Newton* monitoring campaign of the Galactic Centre as well as data from the *ASCA* archive.

2 OBSERVATIONS AND DATA REDUCTION

2.1 *XMM–Newton*

We analysed all *XMM–Newton* (Jansen et al. 2001) observations of AX J1745.6−2901 over the period November 2001 to April 2015. In addition to the observations analysed in Ponti et al. (2015b), we include 10 new *XMM–Newton* observations, taken during outburst (see Table 1 for a full list of *XMM–Newton* observations considered in this work).

We processed the data sets using the latest version (14.0.0) of the *XMM–Newton* Science Analysis System (SAS) and applied the most recent (July 2015) calibrations. We use all the European Photon Imaging Camera (EPIC) (Strüder et al. 2001) cameras. Having higher effective area, our prime instrument is the EPIC-pn (Turner et al. 2001), but we also analysed the EPIC-MOS, for a consistency check. All observations have the medium filter applied and are in Full Frame mode; therefore, the EPIC-pn and EPIC-MOS light curves have minimum time resolutions of 73.4 ms and 2.6 s, respectively. The EPIC pn camera aboard *XMM–Newton* occasionally experiences time jumps. We checked that all the positive and negative jumps are properly corrected by the EPIC-pn reduction pipeline.[1] This is further confirmed by the fact that similar results are obtained with the EPIC-MOS camera that is not affected by these time jumps. The arrival times of all events were corrected to the Solar system barycentre, applying the BARYCEN task of SAS.

Since the main focus of this work is to measure the ingress/egress times and durations of the eclipses, increasing the number of source photons would provide a more accurate determination of the location of the transition points. Therefore, even if photon pile-up significantly affects the brightest observations we decided to retain all source photons (e.g. by not removing photons from the central part of the point spread function as in Ponti et al. 2015a). Pile-up is expected to have a negligible effect on the determination of the eclipse timing. The source and background photons are extracted from circular regions with 40 and 160 arcsec radii, respectively. The former centred on AX J1745.6−2901, while the latter covers a region free from bright point-like sources and low levels of diffuse emission.

For each observation, we identified periods of enhanced particle-induced background activity by inspecting the 6–15 keV source and background light curves binned with 5 s resolution. We filtered out periods with a background level 25 per cent brighter than the average source count rate during the observation. Type I bursts were removed, if clearly detected in 1 s source light curves. We note that type I burst were not detected either at the start, during or at the end of any eclipse.

To establish the X-ray state of the source (see Section 6.3), we used the hardness intensity diagram shown in fig. 2 of Ponti et al. (2015a), based on fluxes in the 3–6 and 6–10 keV bands. When present, pile-up can significantly affect these measurements. To mitigate this we removed (only for this specific analysis) the central 9.25 arcsec in the source extraction region, as done by Ponti, Muñoz-Darias & Fender (2014) and Ponti et al. (2015a). Using the EPIC-pn data with a time resolution of 73.4 ms, we searched for the presence of pulsations during observations with ObsID 0402430301 and 0690441801 (the longest observations where the source is bright in the soft and hard state, respectively) but did not detect any significant pulsed signal.

[1] We checked that all time jumps as well as the unverified deltas and premature increments (see *XMM–Newton* User Handbook, Ebrero et al. 2015) were properly accounted for. During ObsID 0402430401, seven frames (from 4318574 until 4318580) have been repeated; however, this did not produce any time shift. During ObsID 0505670101, two telemetry gaps of 3 s and one of 10 s were observed. Moreover, the quadrant with CCD 4 experienced a negative jump of 3 s, which has been corrected. None of these produced any time shift. During ObsID 0723410501, three gaps of 634.2, 253.2 and 187.8 s, most probably due to telemetry gaps, happened in all CCDs. We manually checked that these intervals were very close to multiple integers of the frame time and that adding or subtracting a one full second time jump would not be multiple integer anymore. Therefore, also these gaps did not produce any time shift.

Table 1. Measured eclipse times of the 29 *XMM–Newton* eclipses and 1 *ASCA* eclipse. The cycle number has been determined with respect to the reference time T_0^e (see Section 4), which is considered to be cycle 0.

ObsID	Cycle number	PN-count rate (counts s^{-1})	Eclipse ingress time[a] (MJD)	Eclipse egress time (MJD)	Error (s)
			ASCA		
52005000	−21561	–	49612.31079	49612.32854	5.1
			XMM–Newton		
0402430701	−8405	9.33	54190.05919	54190.07556	2.2
0402430301	−8400	8.48	54191.79898	54191.81542	2.3
0402430301	−8399	7.52	54192.14693	54192.16335	2.6
0402430301	−8398	6.34	54192.49482	54192.51129	3.0
0402430401	−8394	8.39	54193.88681	54193.90319	2.4
0402430401	−8393	7.95	54194.23470	54194.25111	2.5
0402430401	−8392	6.22	54194.58267	54194.59912	3.0
0505670101	−7374	6.58	54548.80454	54548.82097	2.9
0505670101	−7373	6.46	54549.15253	54549.16899	2.9
0505670101	−7372	6.94	54549.50045	54549.51691	2.8
0724210201	−1666	8.87	56534.95316*	56534.96964	2.2
0724210201	−1665	10.54	56535.30115*	56535.31763	1.9
0700980101	−1636	10.18	56545.39197	56545.40833	2.0
0724210501	−1599	7.41	56558.26641	56558.28280	2.6
0723410301	−1143	1.18	56716.93537	56716.95191	12.3
0723410301	−1142	1.17	56717.28312	56717.29972	12.4
0723410401	−1115	0.81	56726.67793	56726.69466	16.9
0723410401	−1114	0.87	56727.02603	56727.04243	15.9
0723410501	−1050	0.76	56749.29538	56749.31187	17.7
0723410501	−1049	0.89	56749.64329	56749.65972	15.5
0690441801	−1047	0.90	56750.33916	56750.35564	15.4
0690441801	−1046	0.93	56750.68719	56750.70372	15.0
0690441801	−1045	1.02	56751.03514	56751.05157	13.9
0743630201	−617	1.26	56899.96128	56899.97786	11.7
0743630301	−614	1.14	56901.00544	56901.02190	12.7
0743630501	−533	1.18	56929.18989	56929.20639	12.3
0743630601	−101	9.25	57079.50762*	57079.52486	2.2
0743630801	−3	10.59	57113.60843	57113.62483	1.9
0743630901	0	10.91	57114.65233	57114.66868	1.9

[a]Note that some of the ingress times [those marked with asterisk (*)] are affected by the dipping phenomenon, and thus may not be reliable (see discussion in Section 3); we do not provide uncertainties for these measurements, but we expect them to be similar to those estimated for the egress times.

2.2 *ASCA*

To significantly extend the time interval probed by the *XMM–Newton* pointings, we also examined *ASCA* observations. Data were obtained from the HEASARC online data base, and screened event files were used in our analysis. As reported by Maeda et al. (1996), the source was found in outburst in 1993 and 1994. However, no eclipses were found in the 1993 data due to the short duration of the observation (moreover, the source flux was about five times fainter than in 1994). Maeda et al. (1996) reported the discovery of eclipses with a 8.4 h periodicity in the 1994 data. We thus analysed this data set, extracting photons from a radius of 0.8 arcmin as done by Maeda et al. (1996) and combining data from the two Gas Imaging Spectrometers (GIS) instruments, which have a higher time resolution than the SIS. We filtered photons so as to include only those in the 3–10 keV range. Photon arrival times were corrected to the Solar system barycentre using the TIMECONV task of FTOOLS. We found one eclipse fully covered by the observation, in the constructed light curve, which we used for our timing analysis.

Sakano et al. (2001) also reported a detection of the source by *ASCA* in 1997. However, the source flux was significantly weaker in this observation (similar to the levels in 1993), and only a hint of an eclipse was present in their folded light curve. Therefore, we did not include the 1997 data in our analysis.

3 ECLIPSE TIMING

The determination of the eclipse times in all data sets was done using the Bayesian Block technique (Scargle et al. 2013; Ponti et al. 2015c). The technique allows us to detect statistically significant changes in count rates for time-tagged event data, along with a determination of the corresponding times. We first selected the source photons from the cleaned event files and then we applied the Bayesian Block code on the photon arrival times. We performed this on all the data sets. We typically ran the Bayesian Block code over an entire observation, except for observations with intense dipping activity and long exposures, for which we split the event files into smaller segments, each containing one orbital period so that the routine converges in a reasonable amount of time. The eclipse ingress and egress times are singled out without ambiguity by using this technique.

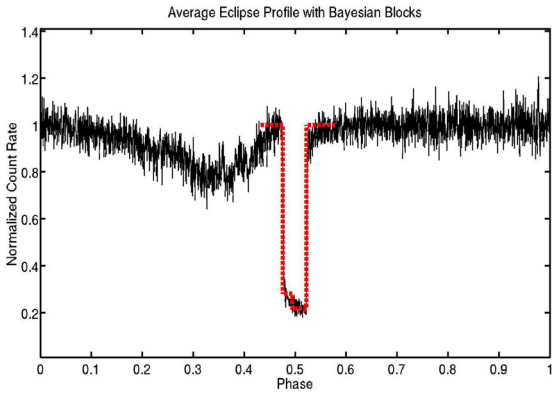

Figure 1. Average, normalized count rate orbital profile in the 3–10 keV band bins are 10 s long. Individual profiles were aligned by using the eclipse centre time (which correspond to phase 0.5) as determined through the analysis described in the text. The red dotted line shows the results of the Bayesian blocks decomposition, at the time of the eclipse, determined during a bright soft state observation. After eclipse ingress a slow residual decay of the flux is observed. The average profile shows that the dipping phenomenon is more intense around phase 0.1–0.5, inducing a significant trough (up to ∼30 per cent) of the average source flux, with a minimum around phase 0.3. Dipping events are sometimes observed just before the start of the eclipse, making the determination of the ingress time less reliable than that of egress time in some orbital cycles.

Fig. 1 shows the average source light curve during one orbit (obtained by averaging over all orbits, after removing type I bursts); phases are defined so that the centre of the eclipse is at 0.5. At the time of eclipse ingress, the source flux abruptly decreases and then it sharply increases again by a similar amount at the time of the egress. Note that during the eclipse, a residual flux is present which displays a gradual decay. It has been suggested that this behaviour is due to a dust scattering halo (Hyodo et al. 2009). In agreement with this interpretation, we observe that the amplitude of this effect steeply decreases at higher energies and is of the same order of magnitude as expected for the large column density to the source ($N_{\rm H} \sim 2 \times 10^{23}$ cm^{-2}; Ponti et al. 2015a). A detailed study of this effect is beyond the scope of this paper.

At low fluxes, most of the observed eclipses are well described by a single block. In these cases, we define ingress and egress times as the start and end times of the block. However, for observations with higher source count rates, the presence of the slow decay during the eclipse induces one additional significant block at the start of the eclipse. Whenever an additional block appears, we define as ingress time, the start of the first block marking the eclipse and as egress time, the end of the last block marking the eclipse (see Fig. 1). By using this method, we determined the start and end times of the 30 eclipses in the data sets that we analysed. Table 1 gives the measured times using this technique.

As a consistency check, we implemented the Bayesian Block technique on event files from the three EPIC cameras separately. Thus, for each eclipse we got three independent measurements of the eclipse times and their Bayesian Block uncertainties. A comparison between the uncertainties determined via the Bayesian Block approximation and those derived directly from the observed scatter (determined considering 12 measurements obtained by the EPIC cameras) suggests that the latter are more reliable (see Appendix and Fig. A1 for details) and therefore were used in the rest of our analysis. In the case of the *ASCA* eclipse, where such a scatter measurement was not possible, we used the uncertainty as inferred from the Bayesian Block algorithm. For measuring the orbital evolution of the system, we used a weighted average[2] of the eclipse times obtained from the three *XMM–Newton* instruments (apart from the eclipse observed by *ASCA*, where we directly used the measured eclipse time from the GIS instrument).

On at least three occasions (cycle numbers −101, −1665 and −1666), we observe that the source was still dipping at the time of the eclipse ingress. Therefore, in order to proceed only with accurate measurements of the transition points, we used only the eclipse egress times to derive the orbital period evolution of the system. We note, however, that the analysis of the ingress times (after rejection of the cycles affected by dipping) provides results which are consistent within the errors of those obtained from egress times.

4 ORBITAL EVOLUTION

The eclipse times determined using the method described above allows us to measure the evolution of the orbital period over an interval of more than 20 yr. We fitted the eclipse egress times with a curve of the form (consistent with a constant orbital period derivative model):

$$T^{\rm e}_N - T^{\rm e}_0 = P_{\rm orb0} N + \frac{1}{2} \dot{P}_{\rm orb0} P_{\rm orb0} N^2 \quad (1)$$

where $T^{\rm e}_N$ is the eclipse egress time, $T^{\rm e}_0$ is the reference eclipse egress time, $T^{\rm e}_0$, $P_{\rm orb0}$ is the orbital period at the epoch $T^{\rm e}_0$, $\dot{P}_{\rm orb0}$ is the constant period derivative and N is the (integer) number of orbital cycle counting from $T^{\rm e}_0$. We choose N to be the closest integer to $(T^{\rm e}_N - T^{\rm e}_0)/P_t$, where P_t is the orbital period estimate given by Hyodo et al. (2009). In each case, we have verified that $|T^{\rm e}_N - (T^{\rm e}_0 + N P_t)| \ll P_t$ to ensure that the number of each orbital cycle is determined without ambiguity.

We first test the possibility of a constant orbital period ($\dot{P}_{\rm orb0} = 0$) through a linear fit. This yields an unacceptable solution with $\chi^2_\nu = 29.1$, indicating that evolution of the orbital period is required by the data. We then used only the eclipse times obtained from *XMM–Newton* observations to determine the ephemeris, and, in particular, to search for an orbital period derivative. We obtain: $P_{\rm orb0} = 30\,063.628 \pm 0.003$ s and $\dot{P}_{\rm orb0} = (-5.1 \pm 1.9) \times 10^{-11}$ s s^{-1}. The reduced χ^2_ν was found to be 3.30 for $\nu = 25$. Thus, a non-zero orbital period derivative for the system was found by using the *XMM–Newton* observations spanning an interval of ∼8 yr (see magenta lines in Fig. 2). We then extended our baseline by more than 10 yr by including now also the *ASCA* observation. The best-fitting parameters are (see also Table 2): $P_{\rm orb0} = 30\,063.6292 \pm 0.0006$ s and $\dot{P}_{\rm orb0} = (-4.03 \pm 0.27) \times 10^{-11}$ s s^{-1}. We now obtain a reduced chi-squared value of $\chi^2_\nu = 3.21$ with $\nu = 26$. We find that the eclipse egress time obtained from the *ASCA* observation, and the best-fitting parameters using all eclipses, agree very closely with the values expected from the orbital solution obtained using solely *XMM–Newton* data (see Fig. 2). This agrees with a unique long-term orbital solution, valid for more than 20 yr. However, we note that, due to the transient nature of the source, the orbital solution is sampled at three epochs; therefore, we cannot exclude a more complex behaviour, such as that observed in EXO 0748–676 (indeed in Sections 5 and 6 evidence for deviations from a unique orbital solution will be presented and discussed). We also test the possibility of a variable $\dot{P}_{\rm orb0}$, by fitting the eclipse times with a

[2] The weights have been taken as the average count rate of the source in the respective instrument during the orbital cycle under consideration.

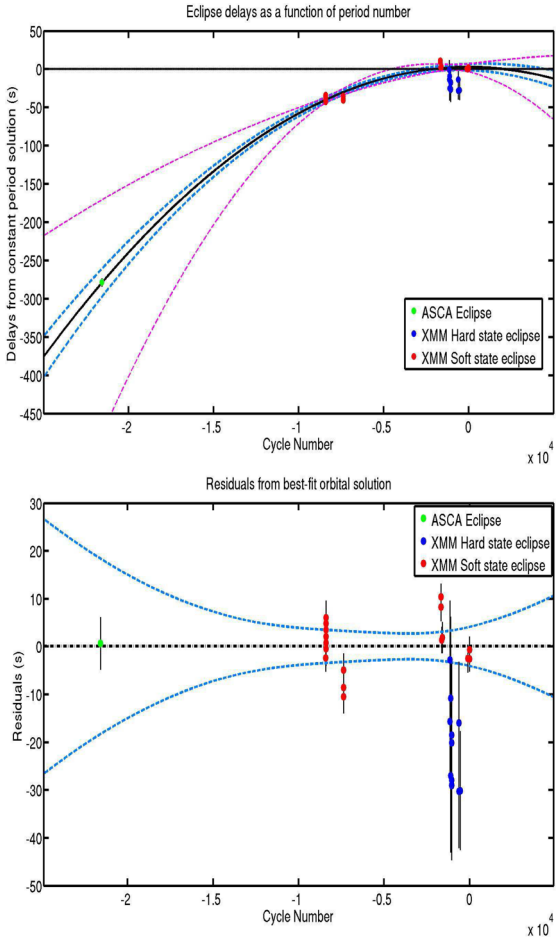

Figure 2. (Top panel) Eclipse time delays (egress times) with respect to a constant orbital period model plotted versus orbital cycle. T_0 (therefore cycle one) corresponds to MJD = 57114.66871. The red and blue circles show the eclipse egress delays corresponding to soft and hard states of the source, respectively, which were observed with *XMM–Newton* whereas the green circle shows the eclipse egress delay derived from the single eclipse in the *ASCA* data (1994). The black solid and blue dashed lines show the best-fitting orbital solution of the combined *XMM–Newton* and *ASCA* data and the 68 per cent confidence region. The magenta dashed lines show the 68 per cent confidence uncertainty on the best-fitting orbital solution obtained by fitting the *XMM–Newton* data only. (Bottom panel) Residuals of the best-fitting orbital solution. Significant scatter is observed.

Table 2. Best-fitting orbital solution for AX J1745.6−2901 derived from the analysis of the eclipse arrival times from 1994 to 2015. Errors are at 1σ confidence level on the last digit. The value of $P_{\rm orb0}$ refers to $T_0^{\rm e}$.

Parameter	Value	Units
$T_0^{\rm e}$	57 114.66871 ± 0.000 05	MJD
$P_{\rm orb0}$	30 063.6292 ± 0.0006	s
$\dot{P}_{\rm orb0}$	−4.03 ± 0.27	10^{-11} s s^{-1}

constant $\ddot{P}_{\rm orb0}$. This results in a $\ddot{P}_{\rm orb0}$ value consistent with 0, and a reduced chi-square value of $\chi^2_\nu = 3.22$, larger than that from the quadratic fit.

The upper panel of Fig. 2 shows the eclipse time delays with respect to a constant orbital period model as a function of orbital cycle. The solid black line shows the best-fitting solution with constant period derivative and the light blue dotted lines the corresponding one sigma uncertainty (the magenta dashed lines show the one sigma uncertainty for the *XMM–Newton* data only). The orbital period of AX J1745.6−2901 clearly evolves in time, shortening by ∼25 ms and producing a delay of ∼300 s over the past 20 yr.

The bottom panel of Fig. 2 shows the residuals compared to the best-fitting model with a quadratic term. Significant residuals, as large as 10–30 s, are observed (see Section 5). In fact the best solution we obtained, with a $\chi^2_\nu = 3.21$ for $\nu = 26$, could be formally rejected because it does not reproduce all the scatter observed in the data. The presence of residual jitter with amplitude comparable to that observed here is typical of eclipsing LMXBs (e.g. Wolff et al. 2009; Jain & Paul 2011). This is discussed further in the next section.

We investigated the reliability of the eclipse timing by applying a different technique to determine the eclipse ingress and egress times. We constructed a model light curve consisting of three parts, corresponding to pre-eclipse, in-eclipse and post-eclipse regions, each with a constant count rate. We then used out a χ^2 minimization routine to fit each of the eclipse light curves (binned to a time resolution of 5 s) to get the corresponding eclipse ingress and egress times for each eclipse. The start and end times of the in-eclipse region would then correspond to the eclipse ingress and egress times. We confirm that the eclipse timings, the orbital solution obtained and the residuals are consistent with that determined using the Bayesian Block analysis.

5 RESIDUAL JITTER

Both the residuals in Fig. 2 and the results of the best fit with a quadratic orbital solution, clearly shows the presence of residual jitter in the eclipse egress time with an amplitude as large as ∼10–30 s. We observe even higher residuals in the ingress time, about ∼50–100 s, when dips are still in progress immediately before the eclipse onset (clearly observed in at least three cases; see Table 1). We interpret them as due to the dipping activity. The smaller jitter in the eclipse egress time is most likely unrelated to dips, because: (i) it is present also during orbits when no dips are detected; (ii) dipping activity is very rarely observed shortly after the eclipse egress. The *XMM–Newton* calibrating team has excluded that the observed jitter has an instrumental origin (private communication).

5.1 State dependence

The top panel of Fig. 3 shows the eclipse ingress as a function of eclipse egress residuals. Note that, in all panels of Fig. 3, the blue (magenta) and red (orange) points refer to the eclipses egress (ingress) time when the source was in the hard and soft state, respectively. A clear correlation between these quantities is observed. Kendall's correlation coefficient is $\tau = 0.91$, with a null hypothesis probability[3] of NHP ∼ 10^{-6}. The presence of such a correlation suggests that the jitter is generated by the eclipses being either delayed or advanced, while their duration remains approximately constant. Indeed, as shown by the bottom panel of Fig. 3, a fit to the observed eclipse durations with a constant provides a reasonable

[3] The null hypothesis is the case where no correlation is present. The NHP provides the probability of the occurrence of such a case. The reported correlation coefficients do not take into account the uncertainties on the data points, that induce scatter, worsening the observed correlation. We do not exclude that the true intrinsic correlation might be slightly better than this estimate.

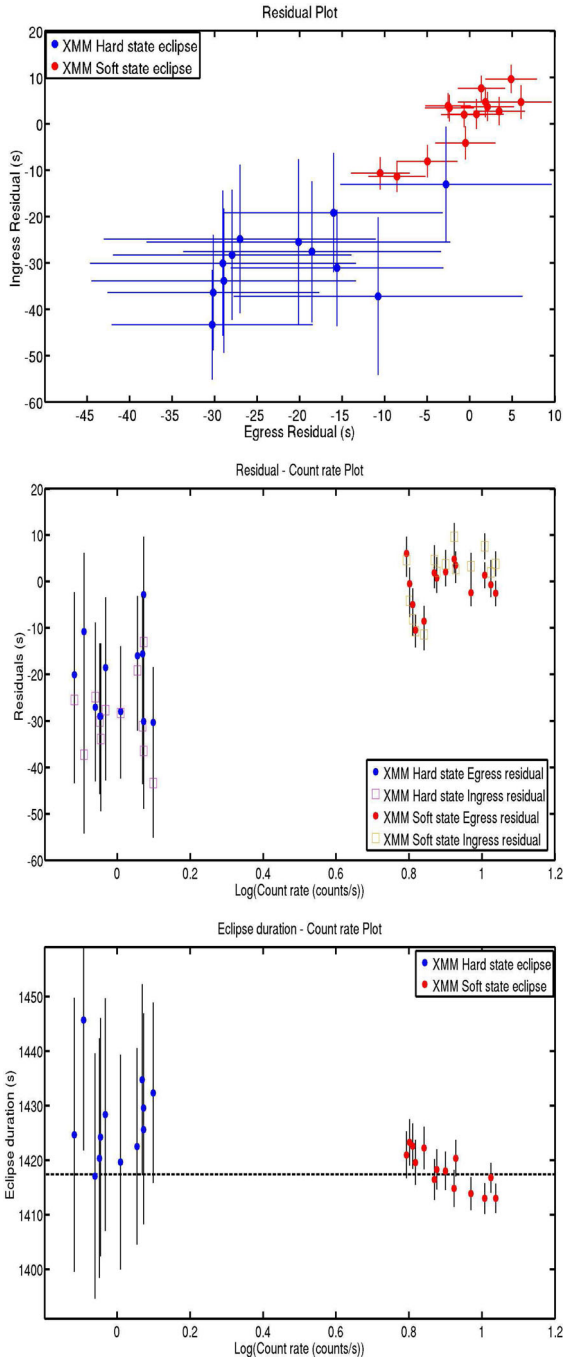

Figure 3. (Top panel) Ingress versus egress time residuals, compared to the best-fitting orbital solution shown in Section 2. Shown here are the 26 eclipses not significantly affected by the dipping phenomenon. The red points show the soft state observations, while the blue points indicate the hard state observations. The residuals in the ingress and egress time are well correlated. (Middle panel) Egress and ingress time residuals as a function of the source count rate with filled circles and open squares, respectively. Soft and hard state observations are shown in red and blue (orange and magenta) for the egress (ingress) times, respectively. Ingress residuals show higher amplitude of variations. (Lower panel) Eclipse duration (defined as eclipse egress time minus eclipse ingress time) as a function of the observed count rate. The variation of the eclipse egress counterbalances the variation of the eclipse ingress, generating an almost constant duration of the eclipse. However, a small, but significant, shortening of the eclipse is observed at high fluxes.

fit ($\chi^2_\nu = 0.774$ for 24 dof; with an average duration of ∼1419.1 s, calculated for eclipses unaffected by dipping). However, we note a trend of decreasing eclipse duration with brightness in the soft state. Considering the duration and count rates during the soft state only, we do indeed observe a hint for a correlation (Kendall's correlation coefficient is $\tau = -0.65$, with a null hypothesis probability of NHP $\sim 7 \times 10^{-4}$). We also note that the eclipse ingress residuals show a higher scatter and span a larger range of values as compared to the egress residuals. This might be related to residual, small amplitude, dipping activity and as a consequence of the decrease of the residual flux due to the dust scattering halo (Jin et al. in preparation).

The top panel of Fig. 3 shows a clear separation between the soft and hard state points. A Kolmogorov–Smirnov test of the distribution of soft and hard state delays (based on the eclipse egress times), indicates that the null hypothesis probability of the two residuals being extracted from the same population is 8×10^{-7}. The state dependence is such that the hard state eclipses in average occur at earlier times (∼29 s) than expected on the basis of the orbital solution. On the other hand, the eclipses happen roughly at the expected time (with an average delay of ∼0.69 s) when the source is in the soft state. This is not surprising because the source is typically brighter (having therefore smaller error bars) during the soft state. The middle and bottom panels of Fig. 3 shows that, indeed, the source is brighter in the soft state and the observed residuals are very well correlated with the source count rate (the Kendall's correlation coefficient is $\tau = 0.5123$, with a null hypothesis probability NHP $\sim 5 \times 10^{-5}$, corresponding to a significance of $\sim 4\sigma$). We note that using the χ^2 minimization technique to determine the eclipse timings also reproduces a clear state-dependence of the residuals (KS null hypothesis probability of $\sim 10^{-4}$), with the residuals being correlated with the source count rate (Kendall's coefficient 0.567, corresponding to a null hypothesis probability of $\sim 10^{-5}$).

6 DISCUSSION

The long-term *XMM–Newton* monitoring of the Galactic Centre joined with archival *ASCA* data allowed us to time the eclipses and measure the evolution of the orbital parameters of AX J1745.6−2901. We fitted the eclipse timing data with a parabolic function, finding a solution valid for more than two decades. In particular, we determined the orbital period of AX J1745.6−2901 with a relative precision of 2×10^{-8}, that is an improvement of over two orders of magnitudes compared to the previous best estimate (Hyodo et al. 2009). We also determine, for the first time, a highly significant decrease of the orbital period of $-4.03 \pm 0.27 \times 10^{-11}$ s s^{-1}, which indicates that the system is shrinking.

We note that, in the best-monitored eclipsing LMXB (EXO 0748−676), eclipse timings obtained over different time intervals do produce inconsistent orbital solutions (Parmar et al. 1986, 1991; Asai et al. 1992; Corbet et al. 1994; Hertz, Wood & Cominsky 1995, 1997; Wolff et al. 2002, 2009). In particular, detailed *RXTE* monitoring of the eclipse timing properties in EXO 0748−676 show that a unique orbital solution can be rejected at high significance and the orbital period evolution can be divided into at least three periods with abrupt changes across them (Wolff et al. 2002, 2009). Interestingly, other eclipsing systems have been suggested to undergo the same erratic behaviour (e.g. XTE J1710−281; Jain & Paul 2011). To check whether this is the case for AX J1745.6−2901, we fitted first the *XMM–Newton* data alone, and then extrapolated the best-fitting orbital solution obtained within the period from 2007

to 2015, to the *ASCA* data from ∼12 yr before (see Section 4). We observe that the same orbital solution fitting the *XMM–Newton* data, with a constant orbital period derivative, intercepts the *ASCA* data (see the magenta dashed lines in Fig. 2). This argues in favour of a unique orbital solution in AX J1745.6−2901 and that the physical mechanism changing the angular momentum in AX J1745.6−2901 is probably different from that at work in EXO 0748−676; however (as a consequence of the sparse temporal sampling), an erratic orbital period evolution is not ruled out.

6.1 Constraints on companion star

By combining the Paczyński (1971) approximate formula for the Roche lobe radius with Kepler's third law, it is possible to derive the average density of the companion star from the system orbital period. Assuming that the companion is a main sequence star, this can be compared with values reported in Cox (2000), which results in $M_2 \simeq 0.8\,\mathrm{M}_\odot$. As often observed in LMXBs, the companion star might be slightly evolved, implying $M_2 \lesssim 0.8\,\mathrm{M}_\odot$. Therefore, the mass ratio is constrained to $q = M_2/M_1 \lesssim 0.6$ for $M_{\rm NS} \geq 1.4\,\mathrm{M}_\odot$.

A low-mass main-sequence star, loosing mass on a time-scale much longer than the time-scale on which the thermal equilibrium is established, is expected to have a mass–radius exponent $n \simeq 0.8$ ($R \simeq M^{0.8}$). When mass-loss is fast (adiabatic), the effective mass–radius exponent is $n \simeq -1/3$ (Rappaport, Joss & Webbink 1982).

6.2 Conservative mass transfer

Conservative mass transfer induced by emission of gravitational waves and magnetic braking can be approximated by

$$\dot{P}_{\rm orb} = -1.4 \times 10^{-14} m_1 m_{2,0.1} m^{-1/3} P_{8\rm h}^{-5/3} \times [1.0 + T_{\rm MB}] \quad (2)$$

$$\times [(n - 1/3)/(n + 5/3 - 0.2 m_{2,0.1} m_1^{-1})]\,\mathrm{s\,s^{-1}} \quad (3)$$

(see Rappaport et al. 1987; Verbunt 1993; Di Salvo et al. 2008; Burderi et al. 2010), where $P_{8\,\rm h}$ is the orbital period in units of 8 h; m_1, $m_{2,\,0.1}$ and m are the mass (in solar masses) of the primary and secondary and binary system ($m_1 + m_2$), respectively (the secondary is expressed in units of $0.1\,\mathrm{M}_\odot$); n is the exponent of the mass–radius relation of the secondary $R_2 \propto M_2^n$, that is assumed to be in the range 0.6–0.8; $T_{\rm MB}$ represents the effects of magnetic braking.

Following and extending the treatment of Burderi et al. (2010; see also Verbunt & Zwaan 1981; King 1988; Verbunt 1993; Tauris 2001; Iaria private communication), we express the magnetic braking term as

$$T_{\rm MB} = 134.4 k_{0.1}^2 f^{-2} m_1^{-1} q^{1/3} (1 + q)^{2/3} P_8^2, \quad (4)$$

where $k_{0.1}^2$ is the quadratic value of the radius of gyration of the star in units of 0.1 (we assume $k = 0.277$, that is $k_{0.1}^2 = 0.767$); f is a dimensionless parameter of order unity with preferred values of $f = 0.73$ (Skumanich 1972) or $f = 1.78$ (Smith 1979). We chose here the value that maximizes the effect of magnetic braking ($f = 0.73$), which results in $T_{\rm MB} = 169$.

We observe that in a conservative scenario the orbital period derivative induced by gravitational radiation alone would be $\dot{P}_{\rm orb} = -1.6 \times 10^{-14}\,\mathrm{s\,s^{-1}}$, while it would be $\dot{P}_{\rm orb} = -6.7 \times 10^{-12}\,\mathrm{s\,s^{-1}}$, if magnetic braking were at work.[4] We note that even the latter estimate is about one order of magnitude smaller than the observed value. We thus conclude that a conservative mass transfer scenario does not reproduce the behaviour of the source. This might be alleviated by non-conservative mass transfer. Indeed, the observation of winds with an outflow rate comparable to or higher than the mass accretion rate (Ponti et al. 2012, 2014, 2015a) in LMXB suggests that the mass transfer rate from the companion star is larger than that implied by conservative mass transfer. If indeed this is the case in AX J1745.6−2901, a faster orbital period evolution might ensue.

Alternatively, the unique orbital solution reliable for more than 20 yr could be a coincidence due to the very sparse sampling concentrated only on three epochs (see Fig. 2). Indeed, it is possible that AX J1745.6−2901 undergoes an erratic orbital period evolution (i.e. Wolff et al. 2009). We note that the observed orbital evolution is of order $\Delta P_{\rm orb}/P_{\rm orb} \sim 10^{-6}$, similar in amplitude to those found in EXO 0748−676, Algol and RS CVn binaries (e.g. Hall 1989). In these systems, the erratic behaviour appears to be due to magnetic activity in the convective envelope of the companion star imparting a torque that changes its gravitational quadrupole moment (Applegate 1992).

6.3 Connection with accretion state

Superposed on the long-term evolution of the orbital period, highly significant jitter (∼10–30 s) is observed. It is unlikely that the residual jitter originates from geometry variations of either the central X-ray source or the inner accretion disc, since these are small and get rapidly eclipsed by the rim of the companion star. In fact, at a velocity of $\sim 390\,\mathrm{km\,s^{-1}}$ (relative to the Neutron Star (NS)], the companion star would swipe through the region where the bulk of the X-ray luminosity is produced, say $\sim 100 r_{\rm g}$ in less than ∼0.7 s (here $r_{\rm g}$ is the gravitational radius defined as $r_{\rm g} = GM/c^2$, where c is the speed of light, G is the gravitational constant and M is the mass of the compact source, assumed to be $1.4\,\mathrm{M}_\odot$).

Applegate (1992) and Applegate & Shaham (1994) proposed a mechanism producing erratic orbital period evolution, based on exchange of angular momentum generated by magnetic activity in the companion star. However, this process typically results in variations on time-scales of years-to-decades and significantly lower amplitudes ($\Delta P_{\rm orb}/P_{\rm orb} \sim 10^{-5,\,-7}$) than those of the observed jitter ($\Delta P_{\rm orb}/P_{\rm orb} \sim 5 \times 10^{-4}$–$10^{-3}$).

It is in theory possible that part of the observed jitter is associated with oscillations of the companion star atmosphere. For example, tidal forces could induce oscillations of the companion star. It is also well known that the magnetic activity in the Sun generates coronal loops extending many thousands kilometres above the photosphere. The presence of such structures above the atmosphere of the companion star may explain the amplitude of the observed jitter. One such event has been claimed in EXO 0748−676 (Wolff, Wood & Ray 2007). However, were such effects at work in AX J1745.6−2901, they would either modify the ingress and egress time in an uncorrelated fashion (in the case of coronal loops), or in an anticorrelated way (i.e. ingress delayed and egress advanced or vice versa, both in case of radial oscillations of the companion star atmosphere or differing irradiation from the central source). Therefore, in all these cases, a variation of the duration of the eclipse, with comparable amplitude to the observed jitter, would be expected. On the contrary, we observe a nearly constant eclipse duration in AX J1745.6−2901.

[4] We note that for a lower exponent of the mass radius relation (e.g. $n = 0.6$ instead of $n = 0.8$), the orbital period evolution is slower, $\dot{P}_{\rm orb} = -4.5 \times 10^{-12}\,\mathrm{s\,s^{-1}}$. In the same way, if the companion is partly evolved and thus has a lower mass (e.g. $m_2 = 0.4$), a slower evolution would be expected, $\dot{P}_{\rm orb} = -2.5 \times 10^{-12}\,\mathrm{s\,s^{-1}}$.

The correlation between ingress and egress residuals suggest that jitter is caused by the whole companion star being either 'delayed' or 'advanced' with respect to the expected long-term orbital period evolution. In particular, the hard state eclipses arrive, on average, ∼29 s before the expected time, while the soft state eclipses arrive very close to the expected time with an average delay of ∼0.69 s. A possibility would be the displacement of the centre of mass of the system, by the presence of a third body. To investigate this, we fitted Doppler shifts in the time of arrival due to the orbital velocity in the presence of a third body in an elliptical orbit (adapting equations from Schreier et al. 1972 and Mukherjee et al. 2006). The sparse sampling of the orbital evolution allows several possible solutions. However, none of these solution is completely satisfactory. Indeed, they either provide an unlikely high eccentricity (higher than 0.999) or predict (unlikely) large residuals ($\Delta t > 60$ s) during the unsampled periods. Moreover, the observed periodicities are multiples of half a year and likely due to the *XMM–Newton* observing window of the Galactic Centre (observable for ∼1.5 months with a cadence of 6 months); therefore, they might be artificial. Moreover, the connection between the eclipse timing and the X-ray source accretion state remains to be explained in the third body interpretation. We can also exclude that the centre of mass could be modified by an asymmetric disc with a state dependent geometry, even though the outer disc bulge, generating dips, is observed to have a state-dependent behaviour. This would require an unrealistically large mass ($\sim 10^{-3}$ $M_\odot$) stored in the bulge to produce the observed jitter.

We note that LMXB typically shows durations of the eclipse transitions (i.e. duration of ingress and egress) of order 5–20 s (Cominsky & Wood 1989; Wachter et al. 2000; Wolff et al. 2009). Interestingly, these are comparable to the jitter observed in AX J1745.6−2901. Transition time-scales are related to the atmospheric scaleheight of the companion star (indeed they correspond to ~ 2–6×10^3 km at a velocity of ∼390 km s^{-1}). AX J1745.6−2901 shows the presence of a highly ionized plasma above the disc, with turbulent velocities of order ∼500 km s^{-1}, temperatures of $kT \sim (4$–$10) \times 10^6$ K and densities of $10^{12\text{–}13}$ cm^{-3} (Ponti et al. 2012, 2014, 2015a). Such ionized plasma might have a thermal origin (Begelman, McKee & Shields 1983; Díaz Trigo et al. 2013; Ponti et al. 2016). Thermal winds originate through irradiation by the central source of the outer disc surface (rotating at the Keplerian velocity). The disc surface heats up as a result of irradiation, thereby raising its thermal velocity. Whenever the thermal velocity exceeds the escape velocity, an outflow is produced. The circularization radius and/or outer disc of AX J1745.6−2901 are characterized by a Keplerian velocity of $v_k \sim 0.75$–1×10^3 km s^{-1} (King, Kolb & Burderi 1996; Muñoz-Darias et al. 2016). We assume that the outflow is launched with the angular momentum characteristic of the outer disc radius and that the plasma travels to the orbit of the companion star without gaining additional angular momentum. If so, it will rotate at a speed of $v_{\rm pl} \sim 170$ km s^{-1}, therefore it will not be in co-rotation with the companion star, which orbits at a speed of ∼390 km s^{-1} (respect to the NS).[5] In these conditions, the plasma will exert a ram pressure on the atmosphere of the star of the order of: $P_{\rm ram} \sim 9 \times 10^2 (n/10^{12}$ cm$^{-3})(\Delta v/220$ km s$^{-1})^2$ dyn cm^{-2}, where n is the plasma density and Δv the velocity difference (assumed to be 10^{12} cm^{-3} and 220 km s^{-1}, respectively). This pressure is comparable to the pressure in the Solar atmosphere at ∼500 km above the photosphere (Cox 2000). Assuming a radial density profile as observed in the Solar atmosphere, we estimate that the eclipse will happen when the line of sight reaches 500–1000 km above the photosphere, where the tangential column density will be $N_{\rm H} \sim 0.3$–5×10^{24} cm^{-2}. Therefore, the ram-pressure induced by the outflow can significantly modify the scaleheight of the companion star atmosphere delaying both the ingress time and the egress time (although to a lesser extent, compared to the ingress time). The eclipse might appear therefore delayed and shortened during the soft state, with the ingress time being more affected than the egress time. No such effect would be present during the hard state, when the disc ionized atmosphere is not present (Ponti et al. 2015a). Although interesting, we note that the amplitudes of the induced delays through this mechanism are of order several seconds, significantly smaller than the observed jitter ($\Delta t \sim 10$–30 s). However, this might be a viable mechanism if the companion star is slightly evolved, therefore having a scaleheight of its atmosphere significantly larger than that of the Sun (Mihalas 1978; Cox 2000; Magic et al. 2013).

We also note that, in this scenario, during the soft state, the ram pressure would act on the companion star, slowing down its motion, and therefore affecting the orbital evolution of the system. This would correspond to an additional contribution to the orbital period evolution of $\dot{P} \sim -3.2 \times 10^{-11}$ s s^{-1} (during the soft state only).

Finally, we note that both the source luminosity and spectral energy distribution change significantly between the two canonical states. In particular, the bottom panel of Fig. 3 shows a correlation between the source count rate and the observed delay. Different levels of irradiation might affect the atmospheric layers of the companion star enhancing mass transfer rate and/or mass-loss (e.g. Tavani 1991).

Moreover, the geometry and physical conditions of the accretion disc are known to be significantly different in the two states. The hard state being characterized by a jet component and an inefficient disc, while the soft state showcasing a standard disc and an ionized atmosphere (Fender et al. 2004; Done, Gierliński & Kubota 2007; Ponti et al. 2012). It appears plausible that different types of outflows, potentially driving away significant amounts of angular momentum and kinetic power, are present in the different states (e.g. jets in the hard state, winds in the soft state; Ponti et al. 2012; Fender & Muñoz-Darias 2016). It is possible that either through irradiation, outflows or other mechanisms the system might lose angular momentum in a different way along the different accretion states.

ACKNOWLEDGEMENTS

The authors wish to thank Ettore Perozzi, Michael Freyberg, Frank Haberl, Matteo Guainazzi and the *XMM–Newton* calibration team for checking that the observed jitter has no instrumental origin. We thank Jan-Uwe Ness, Ignacio de la Calle and the rest of the *XMM–Newton* scheduling team for the enormous support that made the new *XMM–Newton* observations possible. We also thank Barbara De Marco, Thomas Tauris, Jonathan Ferreira, Pierre-Olivier Petrucci, Henri Gilles and Rosario Iaria for very useful discussion as well as the referee for the very useful comments that significantly improved the paper. This research has made use

[5] Assuming a bulk outflow speed of few 10^2 km s^{-1} or lower (Ponti et al. in preparation), for the wind in AX J1745.6−2901, the plasma would require few 10^3 s to reach the orbit of the companion star. At a temperature of $kT \sim (4$–$10) \times 10^6$ K, the speed of the collision between the wind plasma and the atmosphere of the companion star will be close to the sonic point. More meticulous calculations on the details of this idea are deferred to future publications.

primarily of data obtained with *XMM–Newton*, an ESA science mission with instruments and contributions directly funded by ESA Member States and NASA, and on data obtained from the *Chandra* and *ASCA* Data Archives. The GC *XMM–Newton* monitoring project is supported by the Bundesministerium für Wirtschaft und Technologie/Deutsches Zentrum für Luft- und Raumfahrt (BMWI/DLR, FKZ 50 OR 1408 and FKZ 50 OR 1604) and the Max Planck Society. KD would like to thank MPE for the hospitality during his stay, and the German Academic Exchange Service (DAAD) for the fellowship which supported his participation in the project. TMD acknowledges support by the Spanish Ministry of Economy and Competitiveness (MINECO) under the grant AYA2013-42627. LS acknowledges partial support from ASI INAF I/004/11/1.

REFERENCES

Applegate J. H., 1992, ApJ, 385, 621
Applegate J. H., Shaham J., 1994, ApJ, 436, 312
Asai K., Dotani T., Nagase F., Corbet R. H. D., Shaham J., 1992, PASJ, 44, 633
Begelman M. C., McKee C. F., Shields G. A., 1983, ApJ, 271, 70
Burderi L., Di Salvo T., Riggio A., Papitto A., Iaria R., D'Aì A., Menna M. T., 2010, A&A, 515, A44
Chou Y., 2014, Res. Astron. Astrophys., 14, 1367
Cominsky L. R., Wood K. S., 1989, ApJ, 337, 485
Corbet R. H. D., Asai K., Dotani T., Nagase F., 1994, ApJ, 436, L15
Cox A. N., 2000, in Arthur N., ed., Allen's Astrophysical Quantities, 4th edn. Springer-Verlag, Berlin
di Salvo T., Burderi L., Riggio A., Papitto A., Menna M. T., 2008, MNRAS, 389, 1851
Díaz Trigo M., Boirin L., 2013, Acta Polytech., 53, 659
Done C., Gierliński M., Kubota A., 2007, A&AR, 15, 1
Eggleton P. P., 1976, in Eggleton P., Mitton S., Whelan J., eds, Proc. IAU Symp. 73, Structure and Evolution of Close Binary Systems. Reidel, Dordrecht, p. 209
Faulkner J., 1971, ApJ, 170, L99
Fender R., Muñoz-Darias T., 2016, Lecture Notes in Physics, Vol. 905, Astrophysical Black Holes. Springer International Publishing, Switzerland, p. 65
Fender R. P., Belloni T. M., Gallo E., 2004, MNRAS, 355, 1105
Gladstone J., Done C., Gierliński M., 2007, MNRAS, 378, 13
González Hernández J. I., Rebolo R., Casares J., 2012, ApJ, 744, L25
González Hernández J. I., Rebolo R., Casares J., 2014, MNRAS, 438, L21
Hall D. S., 1989, Space Sci. Rev., 50, 219
Hartman J. M. et al., 2008, ApJ, 675, 1468
Hartman J. M., Patruno A., Chakrabarty D., Markwardt C. B., Morgan E. H., van der Klis M., Wijnands R., 2009, ApJ, 702, 1673
Hertz P., Wood K. S., Cominsky L., 1995, ApJ, 438, 385
Hertz P., Wood K. S., Cominsky L. R., 1997, ApJ, 486, 1000
Hu C.-P., Chou Y., Chung Y.-Y., 2008, ApJ, 680, 1405
Hyodo Y., Ueda Y., Yuasa T., Maeda Y., Makishima K., Koyama K., 2009, PASJ, 61, 99
in't Zand J. J. M., Strohmayer T. E., Markwardt C. B., Swank J., 2003, A&A, 409, 659
Jain C., Paul B., 2011, MNRAS, 413, 2
Jain C., Paul B., Dutta A., 2010, MNRAS, 409, 755
Jansen F. et al., 2001, A&A, 365, L1
Kennea J. A., Skinner G. K., 1996, PASJ, 48, L117
King A. R., 1988, QJRAS, 29, 1
King A. R., Kolb U., Burderi L., 1996, ApJ, 464, L127
Knigge C., Baraffe I., Patterson J., 2011, ApJS, 194, 28
Kraft R. P., 1967, ApJ, 150, 551
Kreiner J. M., Ziolkowski J., 1978, Acta Astron., 28, 497
Landau L. D., Lifshitz E. M., 1958, Quantum Mechanics: Non-Relativistic Theory, Vol. 3, 1st edn. Pergamon Press
Lazaridis K. et al., 2011, MNRAS, 414, 3134
Maeda Y., Koyama K., Sakano M., Takeshima T., Yamauchi S., 1996, PASJ, 48, 417
Magic Z., Collet R., Asplund M., Trampedach R., Hayek W., Chiavassa A., Stein R. F., Nordlund Å., 2013, A&A, 557, A26
Mihalas D., 1978, Stellar atmospheres, 2nd edn. Freeman and Co., San Francisco
Mukherjee U., Raichur H., Paul B., Naik S., Bhatt N., 2006, J. Astrophys. Astron., 27, 411
Muñoz-Darias T., Fender R. P., Motta S. E., Belloni T. M., 2014, MNRAS, 443, 3270
Muñoz-Darias T. et al., 2016, Nature, 534, 75
Paczyński B., 1967, Acta Astron., 17, 287
Paczyński B., 1971, ARA&A, 9, 183
Parmar A. N., White N. E., Giommi P., Gottwald M., 1986, ApJ, 308, 199
Parmar A. N., Smale A. P., Verbunt F., Corbet R. H. D., 1991, ApJ, 366, 253
Peters P. C., 1964, Phys. Rev., 136, B1224
Ponti G., Fender R. P., Begelman M. C., Dunn R. J. H., Neilsen J., Coriat M., 2012, MNRAS, 422, L11
Ponti G., Muñoz-Darias T., Fender R. P., 2014, MNRAS, 444, 1829
Ponti G. et al., 2015a, MNRAS, 446, 1536
Ponti G. et al., 2015b, MNRAS, 453, 172
Ponti G. et al., 2015c, MNRAS, 454, 1525
Ponti G., Bianchi S., Muñoz-Darias T., De K., Fender R., Merloni A., 2016, Astron. Nachr., 337, 512
Rappaport S., Joss P. C., Webbink R. F., 1982, ApJ, 254, 616
Rappaport S., Verbunt F., Joss P. C., 1983, ApJ, 275, 713
Rappaport S., Ma C. P., Joss P. C., Nelson L. A., 1987, ApJ, 322, 842
Sakano M., Koyama K., Murakami H., Maeda Y., Yamauchi S., ASCA Galactic Plane /Center Survey Team 2001, in Inoue H., Kunieda H., eds, ASP Conf. Ser. Vol. 251, New Century of X-ray Astronomy. Astron. Soc. Pac., San Francisco, p. 314
Scargle J. D., Norris J. P., Jackson B., Chiang J., 2013, ApJ, 764, 167
Schreier E., Levinson R., Gursky H., Kellogg E., Tananbaum H., Giacconi R., 1972, ApJ, 172, L79
Skumanich A., 1972, ApJ, 171, 565
Smith M. A., 1979, PASP, 91, 737
Soderblom D. R., 1983, ApJS, 53, 1
Staubert R., Klochkov D., Wilms J., 2009, A&A, 500, 883
Strüder L. et al., 2001, A&A, 365, L18
Tauris T. M., 2001, in Podsiadlowski Ph., Rappaport S., King A. R., D'Antona F., Burder L., eds, ASP Conf. Ser. Vol. 229. Evolution of Binary and Multiple Star Systems. Astron. Soc. Pac., San Francisco, p. 145
Tavani M., 1991, Nature, 351, 39
Turner M. J. L. et al., 2001, A&A, 365, L27
Verbunt F., 1993, ARA&A, 31, 93
Verbunt F., Zwaan C., 1981, A&A, 100, L7
Wachter S., Smale A. P., Bailyn C., 2000, ApJ, 534, 367
Wolff M. T., Hertz P., Wood K. S., Ray P. S., Bandyopadhyay R. M., 2002, ApJ, 575, 384
Wolff M. T., Wood K. S., Ray P. S., 2007, ApJ, 668, L151
Wolff M. T., Ray P. S., Wood K. S., Hertz P. L., 2009, ApJS, 183, 156

APPENDIX A: UNCERTAINTIES ON BLOCK CHANGE TIMES

The uncertainty on the block change times (i.e. the eclipses) was first determined using the method suggested in Scargle et al. (2013). This method allows us to compute the probability of change times for each block as a function of the photon arrival times, which peaks at the best-fitting block time. Since the probabilities obtained in this way are discrete, we constructed confidence intervals for change times by calculating the smallest symmetric interval around the best-fitting time which, in total, contains a given confidence level. The reported uncertainties, in all cases, are at a confidence level of

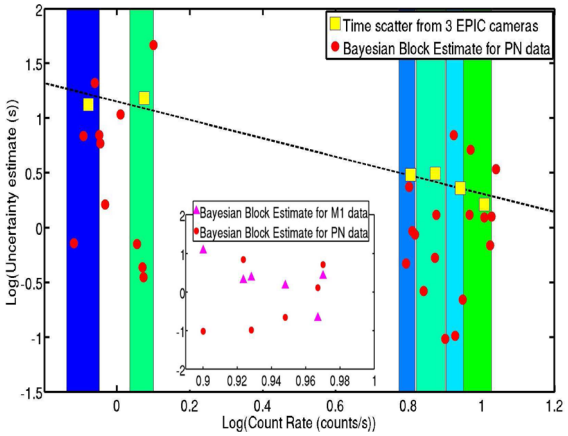

Figure A1. (Main panel) The red circles show the uncertainties on the eclipse egress change times, as observed with the EPIC pn camera, determined through the Bayesian method described in Scargle et al. (2013). The yellow squares show the uncertainties derived from the scatter between the eclipse egress times measured by the different EPIC cameras averaged over orbits with similar sources flux. The coloured vertical regions indicate the flux intervals over which the average is performed. The black dashed line shows the best-fitting relation to the yellow points. (Inset) The red circles and magenta triangles show the uncertainties determined through the Bayesian block method for the EPIC pn and MOS1 cameras, respectively, over a narrow range of observed fluxes. The axes report the same quantities as the main panel.

68 per cent. The red circles in Fig. A1 (both in the main figure and in the inset) show the uncertainties obtained from the EPIC-pn data. The magenta triangles in the inset of Fig. A1 show, instead, the Bayesian block estimates for the MOS1 data. We observe that, for similar source brightness, the uncertainty determined in this way span a range from 0.1 to 7 s, that appears to be relatively large. In particular, unreliably small uncertainties, as small as ∼0.1–0.3 s, are often observed. We note that, as clearly stated in Scargle et al. (2013), this method to determine the uncertainties on the block change times is approximate.

We also estimated the uncertainties based on the observed scatter on the simultaneous observation of the eclipse change points (e.g. egress time) with the three EPIC cameras. The observed scatter (difference between the three measurements of the change times) will be equal to or larger than the intrinsic uncertainty. For each eclipse we define as ingress and egress time the weighted average of the measurements obtained by the three EPIC cameras and we measure the scatter compared to this average. We then sort the eclipses in source mean flux (over the orbital period) and group the eclipses in order to have at least four eclipses in each bin. We finally average the observed scatter over the four eclipses (therefore over a total of 12 data points). The yellow squares in Fig. A1 show the averaged uncertainties obtained in this way. The vertical coloured stripes show the width of the bin over which the scatter has been averaged.

We observe an overall good agreement between the two estimates of the uncertainties. However, we note that the uncertainties derived through the method suggested by Scargle et al. (2013) show a large scatter. In particular, the inset of Fig. A1 reports a comparison between the uncertainty measured by the Bayesian block method from the EPIC-pn and MOS1 data (the axes report the same quantities as the main panel). We observe that on several occasions the MOS1 camera has uncertainties about one order of magnitude smaller than the pn camera, for the same eclipse, despite the smaller effective area. Therefore, we prefer to be conservative and use the second estimate of the uncertainty. We also note that, as expected, the uncertainties are smaller when the source is brighter. We then fit this trend, so that we can associate to any observed source flux an uncertainty on the determination of the change point (see Scargle et al. 2013) and use the latter as uncertainties.

This paper has been typeset from a TEX/LATEX file prepared by the author.